HHS Public Access

Author manuscript

Biochemistry. Author manuscript; available in PMC 2017 March 29.

Published in final edited form as:

Biochemistry. 2016 March 29; 55(12): 1873–1886. doi:10.1021/acs.biochem.6b00067.

Characterization of the Photophysical, Thermodynamic, and Structural Properties of the Terbium(III)–DREAM Complex

Walter G. Gonzalez[†], **Victoria Ramos**[†], **Maurizio Diaz**[‡], **Alyssa Garabedian**[†], **Juan Camilo Molano-Arevalo**[†], **Francisco Fernandez-Lima**[†,§], and **Jaroslava Miksovska**[*,†,§]

[†]Department of Chemistry and Biochemistry, Florida International University, Miami, Florida 33199, United States

[‡]School for Advanced Studies Homestead, Homestead, Florida 33030, United States

[§]Biomolecular Science Institute, Florida International University, Miami, Florida 33199, United States

Abstract

DREAM (also known as K^+ channel interacting protein 3 and calsenilin) is a calcium binding protein and an active modulator of K_V4 channels in neuronal cells as well as a novel Ca^{2+}-regulated transcriptional modulator. DREAM has also been associated with the regulation of Alzheimer's disease through the prevention of presenilin-2 fragmentation. Many interactions of DREAM with its binding partners (Kv4, calmodulin, DNA, and drugs) have been shown to be dependent on calcium. Therefore, understanding the structural changes induced by binding of metals to DREAM is essential for elucidating the mechanism of signal transduction and biological activity of this protein. Here, we show that the fluorescence emission and excitation spectra of the calcium luminescent analogue, Tb^{3+}, are enhanced upon binding to the EF-hands of DREAM due to a mechanism of energy transfer between Trp and Tb^{3+}. We also observe that unlike Tb^{3+}-bound calmodulin, the luminescence lifetime of terbium bound to DREAM decays as a complex multiexponential ($\tau_{average}$ ~ 1.8 ms) that is sensitive to perturbation of the protein structure and drug (NS5806) binding. Using isothermal calorimetry, we have determined that Tb^{3+} binds to at least three sites with high affinity (K_d = 1.8 μM in the presence of Ca^{2+}) and displaces bound Ca^{2+} through an entropically driven mechanism (ΔH ~ 12 kcal mol^{-1}, and $T\Delta S$ ~ 22 kcal mol^{-1}). Furthermore, the hydrophobic probe 1,8-ANS shows that Tb^{3+}, like Ca^{2+}, triggers the exposure of a hydrophobic surface on DREAM, which modulates ligand binding. Analogous to Ca^{2+} binding, Tb^{3+} binding also induces the dimerization of DREAM. Secondary structural analyses using far-UV circular dichroism and trapped ion mobility spectrometry–mass spectrometry reveal that replacement of Ca^{2+} with Tb^{3+} preserves the folding state with minimal changes to the overall structure of DREAM. These findings pave the way for further investigation of the metal binding

[*]**Corresponding Author:** Department of Chemistry and Biochemistry, Florida International University, 11200 SW 8th St., Miami, FL 33199. Phone: 305-3487406. Fax: 305-3483772. miksovsk@fiu.edu.

Supporting Information

The Supporting Information is available free of charge on the ACS Publications website at DOI: 10.1021/acs.biochem.6b00067. Recovered parameters from fitting of the ITC isotherms using an *N*-set-of-sites model (PDF)

Notes

The authors declare no competing financial interest.

properties of DREAM using lanthanides as well as the study of DREAM–protein complexes by lanthanide resonance energy transfer or nuclear magnetic resonance.

Graphical abstract

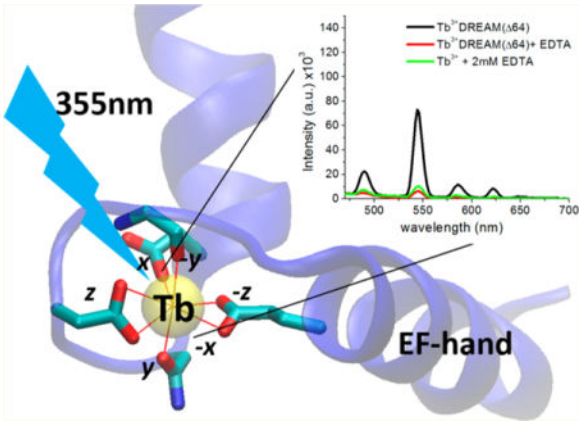

DREAM (downstream regulatory element antagonist modulator), also named KChIP3 and calsenilin, is a 29 kDa multifunctional Ca^{2+}-sensing protein found in different neuronal cell compartments.[1] Outside the nucleus, DREAM interacts with presenilin to regulate amyloid precursor protein processing and with potassium channels to regulate their membrane translocation and gating.[2,3] Moreover, DREAM represents a new class of Ca^{2+}-sensing protein that can translocate to the nucleus and directly bind DNA.[1] In the nucleus, it regulates prodynorphin and c-fos gene expression by binding to the DRE regulatory sequence of those genes.[1,4] Association of DREAM with the DRE promoter regions in the absence of calcium leads to inhibition of gene transcription. These genes have been shown to be involved in apoptosis, cell homeostasis, and pain modulation.[5,6] The role of DREAM in pain sensing, memory retention, learning, and Alzheimer's disease highlights the multifunctional properties of this protein.[6] As a calcium signal transducer, DREAM does not possess endogenous catalytic activity, and its regulatory effect in biological processes arises from interaction with numerous binding partners. Therefore, understanding how calcium and other metals trigger structural changes in DREAM, and how this protein reorganization controls target recognition, would provide important insight into its mechanism of action.

The three-dimensional structure of Ca^{2+}-bound DREAM has been obtained through nuclear magnetic resonance (NMR) and is presented in Figure 1a.[7] DREAM has four EF-hand motifs; EF-hand 3 and EF-hand 4 are able to bind Ca^{2+}, while EF-hand 1 is unable to bind either Mg^{2+} or Ca^{2+}. The coordination of calcium/magnesium in the EF-hand motif has been widely studied, and it has been shown to form hexa- or heptacoordination with oxygen atoms of proteins to form a pentagonal bipyramidal coordination (Figure 1b,c).[8,9] The oxygen-donating amino acids of the calcium selective metal binding loop in EF-hands follow a common organization such that positions 1, 3, and 5 are either an aspartic or an asparagine amino acid while the amino acid at position 12 is a well-conserved glutamic acid (Figure 1b). Modulation of metal affinity and selectivity arises from distinct combinations of negatively charged amino acids at these positions. For instance, EF-hand 2 of DREAM has

been proposed to selectively bind Mg^{2+} due to Glu → Asp mutation at position 12, which eliminates the heptacoordination necessary for strong binding of Ca^{2+}.[10,11] Similarly, the presence of a lysine at position 1, proline at position 5, and aspartic acid at position 12 renders EF-hand 1 of DREAM unable to bind most metals.[10,12]

Association of calcium at the metal binding loop of the active EF-hand pair at the C-terminus of DREAM induces a structural rearrangement that leads to exposure of a hydrophobic surface as well as changes in oligomerization state.[12,13] However, details about the underlying molecular mechanism by which calcium binds and induces structural changes in DREAM are not known. Nonetheless, experiments using NMR to monitor the glycine residues in the EF-hand loops and the associated chemical shift broadening upon metal binding would provide insight into the role of amino acids of DREAM. Of particular interest is the use of lanthanide ions, which have been shown to possess physical properties similar to those of calcium ions and have been widely applied to study the metal binding properties of EF-hands.[14,15] Additionally, lanthanide–protein complexes have been shown to undergo magnetic alignment during NMR experiments, which is of great help in elucidating the three-dimensional structure of protein–metal and protein–protein complexes.[17] The advantage of employing lanthanides to understand the mechanism of calcium binding is their unique luminescence properties as well as their ability to effectively displace calcium from EF-hand loops. Replacement of Ca^{2+} with Tb^{3+} has also been shown to induce structural changes in the EF-hand loops that are highly homologous to those observed upon calcium binding.[16] In this report, we implement a combination of fluorescence, luminescence, TIMS–MS, and calorimetric techniques to show that Tb^{3+} binds at the EF-hands of DREAM and functions as a calcium biomimetic. Moreover, we show that association of Tb^{3+} at EF-hands 3 and 4 of DREAM leads to a calcium-like conformation with hydrophobic surface exposure, oligomeric transition, and ion-neutral collisional cross section (CCS) similar to those observed for the Ca^{2+}-bound protein. Nonetheless, we observe small deviations in the dynamics of the environment near Trp169 as well as secondary structure organization, indicating that not all aspects of Tb^{3+} binding are identical to those of Ca^{2+} binding. Using ITC and the fluorescence properties of Tb^{3+}, we are able to gain insight into the role of Mg^{2+} and ligand binding to DREAM. Initial results of this study have been previously presented in an abstract form.[18]

MATERIALS AND METHODS

General

NS5806 {1-[2,4-dibromo-6-(1*H*-tetrazol-5-yl)-phenyl]-3-(3,5-bis-trifluoromethyl-phenyl)urea, >99% pure} was purchased from Tocris Bioscience, trifluoperazine (TFP) from Sigma-Aldrich, and 1,8-ANS (8-anilino-1-naphthalenesulfonic acid) from Cayman Chemical Co. Concentrated stock solutions were prepared as previously described.[19] $TbCl_3 \cdot 6H_2O$ was obtained from Sigma-Aldrich and used without further purification. Terbium stocks of ~0.5 M were prepared gravimetrically in decalcified ultrapure 18 MΩ water, and the concentrations of Tb^{3+} stocks were confirmed by titrations against EDTA standards.

Isolation and Purification of DREAM Constructs

Recombinant mouse DREAM(Δ64), DREAM(Δ160), and DREAM(Y174A) constructs were expressed in *Escherichia coli* BL21(DE3) cells and purified according to previously published procedures.[12,20] Two additional protein constructs with single-amino acid mutations of glutamic acid at position 12 in the loop of EF-hand 3 and EF-hand 4 were obtained and are named DREAM(E186Q) and DREAM(E234Q), respectively. Rat calmodulin was purified as previously described.[19,21]

Photophysics of the DREAM:Tb^{3+} Complex

Fluorescence experiments were conducted on a custom PC1-ChronosFD instrument (ISS, Champaign, IL) in steady-state mode for excitation and emission spectra and in frequency domain mode for fluorescence decay measurements. The intrinsic protein fluorescence arising from tyrosine residues in CaM and tryptophan on DREAM was obtained by exciting the sample with 280 ± 2 and 295 ± 2 nm light, respectively. The fluorescence of 1,8-ANS was monitored by exciting the sample with 350 ± 4 nm light, through a vertically oriented polarizer. The sensitized emission spectra of terbium(III)-bound proteins were obtained by exciting the sample at 280 ± 4 nm while collecting the emission through a 400 nm long pass filter to minimize the contribution of the protein intrinsic fluorescence and the second harmonic peaks. Displacement of Ca^{2+} from DREAM was monitored by adding small aliquots of a 2.0 mM Tb^{3+} in 20 mM TRIS (pH 7.4) stock solution to 10–20 μM DREAM construct in the same buffer with 5 mM Mg^{2+} and/or 100 μM Ca^{2+}. The resulting spectra were normalized by dividing the intensity at each wavelength by the background value at 530 nm, and the resulting titration plots were fitted using a noncooperative n-site quadratic equation that assumes a similar affinity for all the sites.[20] All spectra were corrected for the PMT wavelength-dependent response as well as the lamp wavelength-dependent changes in intensity. The intrinsic fluorescence lifetime of DREAM was measured by exciting the sample with the modulated light of a 280 nm diode, and the fluorescence collected through a 320 nm long pass filter with 2,5-diphenyloxazole (PPO) in ethanol (τ = 1.40 ns) used a lifetime reference.

Circular dichroism measurements were conducted in a Jasco J-815 CD spectrometer along the 1 mm path of a quartz cuvette (model J-815, Jasco, Easton, MD). Luminescence measurements were conducted on a home-built instrument where the sample was placed in a 2 mm × 10 mm quartz cuvette in a temperature-controlled sample holder (Quantum Northwest, Liberty Lake, WA) and excited along the 10 mm path. The 355 nm line of a Nd:YAG laser (Minilite II Continuum, San Jose, CA) was used to directly excite Tb^{3+} ions, while the luminescence was measured perpendicularly through a 550 ± 10 nm band-pass filter and detected by a H7360-01 PMT (Hamamatsu). The signal was digitized by a 400 MHz oscilloscope (WaveSurfer 42Xs, Teledyne Lecroy), and the initial 100 μs of each trace were deleted to eliminate the contribution from scattered light and PMT recovery time. The fluorescence modulation-phase plots and luminescence decay traces were fit using Globals for spectroscopy software (LFD, Irvine, CA).

Thermodynamics of the DREAM:Tb^{3+} Complex

Isothermal calorimetry titrations were employed to determine the thermodynamics of Tb^{3+} displacement of Ca^{2+} from DREAM or CaM and were conducted using a VP-ITC isothermal calorimeter (Microcal Inc., Northampton, MA). Protein constructs were dialyzed overnight in 5 mM TRIS (Ph 7.4), 100 mM NaCl, and 100 μM $CaCl_2$ with or without 5 mM $MgCl_2$. The use of 10 mM EDTA during purification of calmodulin required multiple overnight dialysis steps to ensure complete removal of contaminating EDTA. Terbium stock solutions were prepared in ITC dialysate buffer. The reaction cell was loaded with an ~10 μM protein solution, determined spectrophotometrically prior to the ITC experiment, and the concentration of Tb^{3+} in the syringe (297 μL) was 1.00 mM. Thirty injections of increasing volume were titrated into the protein solution with increasing time intervals between injections. Isotherms were corrected for the heat of dilution of ligand, and all ITC experiments were conducted in triplicate. The recovered thermodynamic parameters were obtained by fitting the isotherms modeled either with an *N*-set-of-sites model or with a sequential model using the Microcal ITC analysis plug in Origin 7.0.

Trapped Ion Mobility Spectrometry–Mass Spectrometry (TIMS–MS) Studies

Experimental Section—Details regarding the TIMS operation and specifics compared to traditional IMS can be found elsewhere.[22–25] Briefly, in TIMS, mobility separation is based on holding the ions stationary using an electric field against a moving gas. The separation in a TIMS device can be described by the center of the mass frame using the same principles as in a conventional IMS drift tube.[26] The TIMS analyzer was coupled to a maXis Impact Q-UHR-ToF instrument (Bruker Daltonics Inc., Billerica, MA). Data acquisition was controlled using in-house software, written in National Instruments Lab VIEW (2012, version 12.0f3) and synchronized with the maXis Impact acquisition program. TIMS separation was performed using nitrogen as a bath gas at ~300 K, and typical P_1 and P_2 values are 1.8 and 0.6 mbar, respectively. The same RF (880 kHz and 200–350 Vpp) was applied to all electrodes, including the entrance funnel, the mobility separating section, and the exit funnel. Protein samples were prepared at 15 μM protein and 15 μM $TbCl_3 \cdot 6H_2O$ using HPLC grade solvents from Thermo Fisher Scientific Inc. (Waltham, MA) in 10 mM ammonium acetate under physiological conditions (pH 6.7). A custom-built, nano-electrospray ionization source was coupled to the TIMS–MS analyzer and was used for all analyses. A typical source voltage of 600–1200 V was used, and analyses were performed in positive ion mode.

Theoretical—Theoretical CCS were calculated for the previously reported 2JUL NMR structure of DREAM[7] using IMoS (version 1.04b)[27–29] with nitrogen as a bath gas at ~300 K. In the IMoS calculations, 100 total rotations were performed using the diffuse hard sphere scattering method with a Maxwell distribution.

RESULTS

The well-known calcium biomimetic behavior of europium-(III), terbium(III), and neodymium(III) and the unique spectroscopic properties of protein:lanthanide complexes have been widely employed to characterize the sequence of metal binding to calcium

binding proteins,[30–32] to observe protein conformational heterogeneity,[33] to determine water coordination of metals bound at the EF-hand motif,[34] and as binding assays.[35] Therefore, we envisioned that the properties of lanthanides could be employed to obtain information about the biophysical properties of DREAM protein. However, the association of lanthanides with the KChIP subfamily of calcium binding proteins has not been extensively studied. Thus, we first set forth to determine whether Tb^{3+} can directly associate with the EF-hand of DREAM. This is important, because previous studies of DREAM(Δ64) using mass spectrometry and studies of NCS-1 using sensitized emission have presented contradicting results on whether Tb^{3+} can bind to neuronal calcium sensors.[10,36] Additionally, we are interested in investigating whether Tb^{3+} binding induces structural changes in DREAM homologous similar to those observed for calcium.

Terbium(III) Binds to DREAM and Is Sensitized by Energy Transfer from W169

Calmodulin and DREAM are well-known to undergo distinct structural changes upon binding of calcium, which are accompanied by changes in fluorescence of tyrosine and tryptophan residues, respectively.[1,37] These fluorescence transitions are shown in panels a and b of Figure 2. When calcium binds, the tyrosine fluorescence of CaM increases whereas the tryptophan fluorescence of DREAM decreases, in agreement with previous reports. Of particular interest is the observation that in the presence of Tb^{3+}, at molar ratios of 4:1 for CaM and 2:1 for DREAM, the fluorescence emission is nearly identical to that observed in the presence of saturating calcium (Figure 2a,b). The slightly lower tyrosine fluorescence of CaM in the presence of Tb^{3+} is likely due to an efficient quenching of Tb^{3+} by an aromatic amino acid or due to incomplete binding of this ion. We also investigated whether binding of Tb^{3+} on DREAM leads to the transfer of energy from nearby aromatic residues toward the metal ligand, as previously observed for CaM.[32] The presence of the characteristic sharp emission bands in the sensitized emission spectra of the DREAM(Δ64):Tb^{3+} complex supports the idea that aromatic residues, likely at the C-terminus of DREAM, are able to transfer energy to bound terbium (Figure 2c,d). The sensitized emission intensity of terbium bound to DREAM(Δ64) is approximately half of that observed for CaM, which is likely due to the presence of only two Tb^{3+} ions bound to EF-hands 3 and 4 of DREAM(Δ64), whereas four Tb^{3+} ions are bound to CaM.[10] Nonetheless, it is also possible that the presence of Tyr100 at position 7 of the EF-hand 3 binding loop and Tyr139 at position 10 of EF-hand 4 on CaM provides a more efficient energy transfer to Tb^{3+}.[38]

Detailed analysis of DREAM(Δ64) excitation spectra due to the $^5D_4 \rightarrow {}^7F_5$ transition at 545 nm shows a broad peak with maxima at 280 and 32 nm fwhm (Figure 3a). The ratio of terbium luminescence intensity upon excitation at 295 and 280 nm is 0.40, which indicates that tyrosine and tryptophan residues are able to transfer energy.[39] The excitation spectra of DREAM(Δ160), DREAM(E186Q), and DREAM(E234Q) are identical to those of DREAM(Δ64), with a broader fwhm of 36 nm and a higher 295 nm/280 nm ratio of 0.52 for DREAM(Δ161). Analysis of the C-terminal domain of DREAM shows the presence of three tyrosine residues (Y174, Y195, and Y203); however, only Y174 is within the range of 5–10 Å necessary for an efficient energy transfer to Tb^{3+} bound at EF-hands 3 and 4 (Figure 3b).[40,41] Therefore, to quantify the energy transfer contribution of Y174, we constructed a DREAM(Y174A) mutant and determined the effect of this mutation on the sensitized

emission and excitation spectra. This mutant shows an identical circular dichroism transition and amplitude as well as the same Tb^{3+}-induced tryptophan fluorescence change, as the DREAM(Δ64) construct (data not shown). On the other hand, the efficiency of energy transfer in the DREAM(Y174A) mutant is decreased by ~60%, judging from the decreased sensitized emission at 545 nm (Figure 3a). The excitation spectra of this construct also show a 5 nm blue shift to 275 nm with a fwhm of 38 nm and a 295 nm/280 nm ratio of 0.41. The decrease in the sensitized emission and the blue shift of the excitation spectra support the role of Y174 as an energy donor, while the identical 295 nm/280 nm ratio for DREAM(Δ64) and DREAM-(Y174A) is indicative of Tyr → Trp → Tb^{3+} being the predominant energy transfer pathway. The similar Tb^{3+} sensitization observed in DREAM(Δ161) and DREAM(Δ64) constructs indicates that aromatic amino acids at the N-terminus do not transfer energy to Tb^{3+} and that the observed luminescence arises from terbium bound at EF-hands 3 and 4. For comparison, the excitation spectra of CaM are also shown, and a characteristic maximum at 277 nm with fwhm of 24 nm and a 295 nm/280 nm ratio of 0.07 is observed, which is in good agreement with a Tyr → Tb^{3+} energy transfer. Moreover, the lack of vibronic structures on the excitation spectra on all constructs indicates that phenylalanine residues do not play a major role in energy transfer.

The shorter distance from Tyr174 to EF-hand 3 (10.5 Å) than to EF-hand 4 (13.5 Å) supports the idea that monitoring the binding of Tb^{3+} using the sensitized emission may allow us to identify whether aromatic amino acids on DREAM can transfer energy to Tb^{3+} bound at both EF-hands. To confirm this hypothesis, we employed two DREAM constructs in which glutamic acid at position 12 of the calcium binding loop has been mutated to glutamine, thus inactivating either EF-hand 3 in DREAM(E186Q) or EF-hand 4 in DREAM(E234Q).[42] As expected, the excitation spectra of Tb^{3+} bound at EF-hand 3 in the DREAM(E234Q) mutant shows fluorescence ~39% greater than that of Tb^{3+} bound at EF-hand 4 in the DREAM(E186Q) mutant (Figure 3a).

Titration of Tb^{3+} into Ca^{2+}-bound DREAM(Δ64) or DREAM(Δ161) shows that both construct have a similar affinity for Tb^{3+} in the presence of calcium. The dissociation constant obtained using the quadratic equation shows identical affinity for Tb^{3+} in the presence of Ca^{2+} with a K_d of 1.8 ± 0.6 μM for DREAM(Δ64) and a K_d of 1.6 ± 0.2 μM for DREAM(Δ161). Interestingly, in the presence of 5 mM $MgCl_2$, the sensitized emission of Tb^{3+} is decreased by 53% for DREAM(Δ64) but no significant changes are observed for DREAM(Δ161) (Figure 3c). To better understand the mechanism of binding of Tb^{3+} to EF-hands 3 and 4 of DREAM, we have also conducted titrations in the presence of Ca^{2+} or Mg^{2+} and Ca^{2+} using the DREAM(E186Q) and DREAM(E234Q) protein mutants (Figure 3d). Displacement of Ca^{2+} from DREAM(E186Q) by Tb^{3+} shows a weaker dissociation constant of 11 ± 1 μM compared to that of DREAM(E234Q) (5.9 ± 0.5 μM). However, a decrease in the sensitized emission upon addition of 5 mM $MgCl_2$ similar to that for DREAM(Δ64) was observed, with emission decreases of 55 and 80% for DREAM(E234Q) and DREAM(E186Q), respectively (Figure 3d). Under the conditions used for these titrations (500 μM $CaCl_2$ or 500 μM $CaCl_2$ and 5 mM $MgCl_2$), Tb^{3+} binds first to the inactivated EF-hand (see ITC experiments below). Therefore, the data shown in Figure 3d highlight the fact that binding of Mg^{2+} to EF-hand 2 induces structural rearrangements that have a greater impact on EF-hand 3. This is in good agreement with the fact that EF-hand 2

is adjacent to EF-hand 3, and that the exiting helix of EF-hand 2 is in direct contact with the entering helix of EF-hand 3 (Figure 1a). Tryptophan 169 and tyrosine 174, both of which are shown to play a major role in energy transfer, both reside on the entering helix of EF-hand 3. The presence of Mg^{2+} also enhanced the binding of Tb^{3+}, with dissociation constants of 5.8 ± 1.9 μM for DREAM(E186Q) and 2.7 ± 0.4 μM for DREAM(E234Q). This increase in apparent affinity is likely due to a decrease in the level of nonspecific binding of Tb^{3+} to secondary sites or to EF-hand 2. Together, these results support a model in which terbium displaces Ca^{2+} from EF-hand 4 and EF-hand 3 and highlight the role of Mg^{2+} binding at EF-hand 2 as a structural cofactor in DREAM.

Binding of Terbium(III) to DREAM Leads to a Structural Rearrangement Similar to Those Observed for Ca^{2+}

The terbium(III)-induced tryptophan emission quenching observed in Figure 2b supports the idea that Tb^{3+} is able to mimic the structural changes induced by binding of Ca^{2+} to EF-hands 3 and 4. To test whether binding of Tb^{3+} to DREAM induces a structural transition analogous to that of Ca^{2+}, we monitored the fluorescence and anisotropy decay of Trp169, the fluorescence of the extrinsic hydrophobic probe 1,8-ANS bound at the C-terminus of DREAM(Δ64),[13] and changes in secondary structure. Detailed information regarding the environment and dynamics of Trp169 and how they are affected by metal binding can be obtained by measuring the fluorescence and anisotropy decay lifetimes. As previously reported,[43] the fluorescence decay of Trp169 on DREAM-(Δ64) was best fitted by a Gaussian-discrete bimodal decay model, whose parameters are listed in Table 1 and shown in Figure 4a. The small discrepancies between our results and those published previously likely arise from the lack of LDAO detergent under our conditions. Nonetheless, we observe that addition of Ca^{2+} or Tb^{3+} results in a decrease in the average excited-state lifetime from 4.8 to 3.8 ns, which is due to a decrease in the fractional intensity contribution of the long lifetime and a slightly faster Gaussian decay from 1.8 to 1.5 ns. The lack of significant lifetime quenching of Trp169 by Tb^{3+} is likely due to the poor efficiency of this energy transfer process. Moreover, anisotropy decay measurements were conducted to identify whether binding of Tb^{3+} induces dimerization of DREAM as observed for Ca^{2+}. The frequency domain anisotropy decay data were best fitted with a double discrete model, in which the fast Θ_1 is associated with fast local fluctuations of tryptophan and the slow Θ_2 corresponds to the global rotation of the protein (Table 1). A clear transition from 15 to 29 ns upon binding of Ca^{2+} and 27 ns in the presence of Tb^{3+} is observed. These rotational correlation times match well with the values of 14 ns for a monomeric and 28 ns for a dimeric DREAM(Δ64) protein approximated by the Einstein–Stokes equation at 17 °C, η = 0.0100 P, and 0.73 g/mL hydration. Differences in rotational correlation times of the fast local tryptophan motion can be observed between Ca^{2+}- and Tb^{3+}-bound DREAM(Δ64), where a 2-fold faster local motion is measured in the presence of terbium (0.52 ns vs 0.23 ns). In the metal-free DREAM(Δ64), the local flexibility accounts for 35% of the depolarization, while in the Ca^{2+}- and Tb^{3+}-bound DREAM(Δ64) form, this rotation contributes 48 and 58% to depolarization, respectively. Altogether, excited-state and anisotropy decay of Trp169 reveals that even though binding of Tb^{3+} can induce dimerization of DREAM(Δ64) this metal also induces a more dynamic structure near the Trp169 compared to Ca^{2+}.

As shown in Figure 4b, the CD spectrum of metal-free DREAM(Δ64) shows a characteristic profile with minima at 222 and 208 nm (the maximum at 190 nm is not shown) in good agreement with an α-helical structure. Upon binding of Ca^{2+}, an ellipticity decrease at 200–225 nm and an increase at 190 nm are observed, which can be explained by an increase in α-helical content and/or rearrangement of the α-helices. On the other hand, in the presence of Tb^{3+}, a CD spectrum intermediate between those measured for apo and Ca^{2+}-bound DREAM is observed. This intermediate structure was also observed when a 2-fold excess of terbium was added to a sample containing 100 μM calcium (not shown). The largest deviation in CD spectra between Ca^{2+}- and Tb^{3+}-bound DREAM(Δ64) is observed near the 208 nm minimum. Thus, the CD data indicate that Tb^{3+} is able to displace Ca^{2+} and induce a structural change distinct from those observed for metal-free and Ca^{2+}-bound DREAM(Δ64).

Despite the small differences in the protein dynamics near Trp169, as well as the deviation in secondary structure upon binding of Tb^{3+}, we observed similar binding of 1,8-ANS at the C-terminal hydrophobic cavity of DREAM(Δ64).[13] The fluorescence emission of this probe has been extensively shown to be sensitive to the immediate environment, and while the total intensity upon Ca^{2+} binding is observed to increase, no changes in fluorescence of 1,8-ANS were observed upon displacement of Ca^{2+} by Tb^{3+} (Figure 4c). Moreover, frequency domain analysis of the excited state of 1,8-ANS as well as the depolarization time reveals no significant differences between Ca^{2+}- and Tb^{3+}-bound DREAM(Δ64) (data not shown). Overall, the indication is that the hydrophobic cavity exposure induced by calcium is also triggered by terbium.

DREAM Binds Tb^{3+} through an Entropy-Driven Mechanism

To complement the Tb^{3+}:DREAM binding studies using sensitized emission, we also conducted calorimetric studies in which the heat associated with Tb^{3+} displacement of Ca^{2+} bound at the EF-hands of CaM and DREAM is measured. Isothermal calorimetry reveals that displacement of Ca^{2+} from CaM is endothermic and can be best modeled as a sequential process (Figure 5a). The profile of the ITC isotherm for Tb^{3+} displacement of Ca^{2+} bound to CaM is similar to that obtained for binding of calcium to a plant–mammalian CaM chimera,[44] albeit with slightly different thermodynamic parameters. The associations of Tb^{3+} ions with CaM at EF-hands 1–4 have association constants slightly lower than those determined for Ca^{2+} binding, which is likely due to competition effects. We associate the site with K_1 parameters as representing the displacement of Ca^{2+} by Tb^{3+}, while the two other observed binding processes (K_2 and K_3) likely arise from a convolution of specific and nonspecific association of Tb^{3+} ions. The presence of nonspecific binding of Tb^{3+} ions is supported by the fact that addition of 5 mM Mg^{2+} results in drastic changes in the thermodynamic parameters associated with K_2 and K_3. The observed decreases in enthalpy and entropy of ~160 and ~280 kcal mol^{-1} for K_2 and K_3, respectively, also support the idea that these supplementary sites are strikingly different and may involve different ligands and/or ion displacement. We associate the thermodynamic values recovered in the presence of Mg^{2+} with the displacement of Ca^{2+} specifically bound at the loops of EF-hands 1–4, convoluted with any additional protein rearrangement to accommodate Tb^{3+}. It can be observed that in the presence of Mg^{2+} there is a 3-fold decrease in affinity for the K_1 site,

with a minimal change in enthalpy and entropy, whereas sites K_2 and K_3 show similar affinity, with K_2 having an enthalpy and entropy 2-fold larger than those of K_3 sites. Altogether, these values can be interpreted as corresponding to Tb^{3+} displacement of Ca^{2+} ions from four EF-hands with K_1 representing the weakest Ca^{2+} binding hand and K_2 and K_3 corresponding to the three remaining EF-hands. Following previous studies in which calmodulin was shown to follow a sequential filling of EF-hands 1 → 2 → 3 and 4 by Tb^{3+} and Ca^{2+}, we associate the K_1 binding site to that of binding of Tb^{3+} to EF-hand 4.[32,45] Interestingly, EF-hand 4 in calmodulin shows the presence of glutamic acid at position 11 near the $-z$ metal coordination (Figure 1), which may explain the smaller enthalpic and entropic contribution upon displacement of Ca^{2+} by Tb^{3+}. The Tb^{3+} binding sites corresponding to K_2 show ΔH_2 and ΔS_2 thermodynamic parameters that are ~2-fold larger than those of ΔH_3 and ΔS_3, which is likely due to two Tb^{3+} binding sites being reported by the K_2 parameters. This allows us to approximate a ΔH value of ~23 kcal mol^{-1} and a $T\Delta S$ of ~27 kcal mol^{-1} for Tb^{3+} displacement of Ca^{2+} bound at EF-hands 1–3 and a ΔH of 13 kcal mol^{-1} and a $T\Delta S$ of 28 kcal mol^{-1} for EF-hand 4.

Furthermore, displacement of Ca^{2+} bound to DREAM(Δ64) by Tb^{3+} shows a simpler isotherm (Figure 5b), which is similar to that obtained for displacement of Ca^{2+} by Tm^{3+} in the *Entamoeba histolytica* calcium binding protein.[14] Despite the ability to model the isotherm using the simpler one-set-of-sites model, we decided to present the results obtained from a three-site sequential model based on three accounts. First, it is expected that binding of Tb^{3+} is not associated with a cooperative behavior because the protein undergoes a transition from a calcium-bound structure to a calcium-like structure. Second, replacement of glutamic acid at position 12 of the loop in EF-hand 3 resulted in an isotherm that could not be fitted by a one-set-of-sites model. Lastly, displacement of Ca^{2+} by Tb^{3+} in other calcium binding proteins with known calcium cooperativity have been observed to follow a sequential mechanism.[14,44] The recovered parameters using the sequential model are listed in Table 2. For the sake of completeness, the parameters recovered with an *N*-set-of-sites model are presented in Table S1. The data reveal that three Tb^{3+} ions can bind to DREAM(Δ64), with slightly different affinities, such that $K_1 > K_2 > K_3$. Interestingly, the associated enthalpy and entropy of sites K_1 and K_2 are similar to those found for Ca^{2+} displacement of K_1 sites on CaM, while the enthalpy and entropy of the site corresponding to K_3 show significantly lower enthalpic and entropic contributions. Titration of Tb^{3+} in the presence of Ca^{2+} and 5 mM Mg^{2+} in DREAM(Δ64) increases $\Delta\Delta H_3$ and $T\Delta\Delta S_3$ by ~6 kcal mol^{-1}, while the enthalpy and entropy of sites K_1 and K_2 remain unchanged. Unlike CaM, in which all four EF-hands are believed to prefer binding to Ca^{2+} versus Mg^{2+}, EF-hand 2 on DREAM is proposed to bind Mg^{2+} preferentially.[8,10] Therefore, we assign the recovered thermodynamic parameters for sites with K_1 and K_2 association constants as representing Ca^{2+} displacement from EF-hand 3 or 4 while those recovered for the site with K_3 being representative of binding of Tb^{3+} to EF-hand 2. The assignment of K_3 to EF-hand 2 is also supported by the displacement of Ca^{2+} by Tb^{3+} in a DREAM(Δ160) construct lacking the Mg^{2+} binding EF-hand 2, which shows only two sites with affinities and thermodynamic parameters similar to those of K_1 and K_2 on DREAM(Δ64). The recovered association constant and thermodynamic parameter for binding of Tb^{3+} to DREAM-(Δ160) are also independent of Mg^{2+}, in agreement with the sensitized emission titrations. However, despite

the similarities, a decrease of ~10 kcal mol^{-1} in the enthalpy and entropy for the K_2 site is observed for DREAM(Δ160) compared to that of DREAM(Δ64). This decrease in energetics could be due to a distinct metal coordination or loss of structural rearrangement at the missing N-terminus. It is tempting to assign the K_2 parameters of DREAM(Δ160) as representing binding of Tb^{3+} to EF-hand 3, due to closer proximity to the now deleted N-terminal domain, but these results do not permit unequivocal assignment. Together, the recovered thermodynamic parameters for DREAM(Δ64) and DREAM(Δ160) show that Tb^{3+} can efficiently displace Ca^{2+} from the C-terminal EF-hands 3 and 4, and that deletion of the N-terminal amino acids (1–160) results in modification of the metal binding properties of EF-hands 3 and 4. Thus, we can approximate a ΔH value of ~15 kcal mol^{-1} and a $T\Delta S$ of ~22 kcal mol^{-1} for Tb^{3+} displacement of Ca^{2+} bound at EF-hands 3 and 4 of DREAM(Δ64).

Additional experiments in which we monitored the thermodynamics of association of Tb^{3+} with Ca^{2+}-bound DREAM(E186Q) with inactivated EF-hand 3 and DREAM(E234Q) with inactivated EF-hand 4 were also conducted, and the recovered parameters are listed in Table 2. Displacement of Ca^{2+} by Tb^{3+} on the DREAM(E186Q) construct is best modeled as a three-site sequential binding process, in which the K_1 site has the highest affinity, while ΔH_1 and ΔS_1 are ~5 kcal mol^{-1} lower than those obtained for DREAM(Δ64). Tb^{3+} binding at the site with K_2 shows an affinity identical to that observed for K_2 on DREAM(Δ64) in the presence of Mg^{2+}, and similar enthalpic and entropic contributions. The third site, K_3, shows parameters similar to those recovered for Tb^{3+} binding at EF-hand 2 of DREAM(Δ64) and likely corresponds to the same binding process. The decrease in enthalpy and entropy upon binding of Tb^{3+} at the site with K_1 as well as its stronger binding affinity compared to those of K_2 and K_3 seems to indicate that this site likely corresponds to the inactivated EF-hand 3. The fact that only small changes are observed upon mutation of glutamic acid at position 12 ($-z$ coordination) to glutamine supports the idea that this site may still be weakly bound to either Ca^{2+} or Mg^{2+}. Interestingly, these results also show that the E186Q substitution does not affect the binding of Tb^{3+} at EF-hand 3, which is interesting but not unexpected. This effect is likely due to weaker binding of Ca^{2+}, which in turn facilitates Tb^{3+} association.

The DREAM(E234Q) construct, in which EF-hand 4 is inactivated, is also able to bind three Tb^{3+} ions with ranges of affinities similar to those obtained for the DREAM(Δ64) in the presence of Mg^{2+}. In this construct, the site with association constant K_2 binds stronger, followed by K_3 and then K_1 sites. However, the enthalpy for site K_2 on DREAM(E234Q) is 5-fold lower than those obtained for K_2 on DREAM(Δ64). The sites with a K_3 association constant show an enthalpy and an entropy identical to those of the site corresponding to K_3 on DREAM(Δ64). In fact, the enthalpy and entropy for sites K_2 and K_3 are much closer to those obtained for binding of Tb^{3+} to EF-hand 2 of DREAM(Δ64) in the presence of Mg^{2+}, with a ΔH of ~4 kcal mol^{-1} and a ΔS of ~10 kcal mol^{-1}. These results suggest that inactivation of EF-hand 4 likely results in a weak binding of Ca^{2+} or Mg^{2+}, both of which can be easily displaced by Tb^{3+} (based on higher K_2 and K_3) with a concomitant lower enthalpic and entropic contribution. Overall, ITC demonstrates that in the presence of saturating amounts of calcium, the Glu → Gln mutation at position 12 of the EF-hand metal binding loop actually facilitates binding of Tb^{3+}.

Luminescence Decay of Tb^{3+}-Bound DREAM Is Sensitive to Ligand Binding

Sensitized emission studies show that Mg^{2+} is able to induce changes in the emission of bound Tb^{3+}; to further study this effect, we decided to determine if Mg^{2+} can induce structural changes within the coordination sphere of Tb^{3+}. We employed direct excitation of Tb^{3+} using the 355 nm line of a Nd:YAG pulsed laser and measured the luminescence decay of terbium bound to the EF-hands of CaM and DREAM constructs. This approach permits analysis of the local environment at the binding site of Tb^{3+} ions, namely the EF-hand loops. Additionally, this method has been widely used to monitor changes in the coordination sphere of lanthanides as well as the effects of water coordination.[46] Following the studies described above, we first characterized the luminescence decay of Tb^{3+} bound to CaM, and as expected, the luminescence decay shown in Figure 6a follows a monoexponential decay with a τ_1 of 1.38 ms. A single-exponential decay of approximately 1 ms has been reported for the Tb^{3+}:CaM complex, and double-exponential decays have been observed for complexes of Eu^{3+} and calmodulin.[30,33]

Luminescence decay of Tb^{3+} bound to DREAM(Δ64) shows a τ_1 lifetime of 0.86 ms (59%) and a τ_2 lifetime of 2.20 ms (14%), whereas Tb^{3+} bound to DREAM(Δ160) decays with a τ_1 lifetime of 0.74 ms (54%) and a τ_2 lifetime of 2.16 ms (29%). The faster lifetime likely corresponds to a contribution from partially coordinated Tb^{3+} ions and is similar to the 780 μs decay obtained for Tb^{3+} bound to NTA in water.[34] We and others have determined the lifetime of Tb^{3+} in buffer at pH 7.4 to be 450 ± 30 μs; therefore, we associate τ_1 to represent Tb^{3+} bound to a weak coordination site on DREAM.[47] The second lifetime is much longer than that determined for Tb^{3+} bound to parvalbumin (1.3 ms) or CaM (1.38 ms) but is similar to that of Eu^{3+} bound to these proteins or complexes of Tb^{3+} and bimetallic ligand in which no water coordination is observed.[30,34,48] Long-lived excited-state decays are observed for lanthanides with little phonon quenching that often is due to limited water access.[47] Interestingly, addition of 100 mM NaCl reduces the fast lifetime to values similar to those of Tb^{3+} in water and increases the fractional intensity of the long lifetime component ~3-fold (Table 3). The luminescence decay of Tb^{3+} was not significantly affected by LDAO, a detergent that has been proposed to stabilize DREAM in a single conformation.[12] Titration of Tb^{3+} into DREAM(Δ64) in the presence of 100 mM NaCl and 10 mM LDAO shows that the fractional intensity of the τ_2 lifetime increases in a dose-dependent manner and saturates at a stoichiometric ratio of 2:1, whereas the fractional intensity of τ_1 decreases (Figure 6b,c).

Additional measurements of the luminescence decay of the DREAM construct with inactivated EF-hands show similar bimodal exponential decays. One of the most salient observations is that the decay lifetime of DREAM(E234Q) is significantly shorter [τ_2 = 1.75 ms (27%)] than that observed for DREAM(E186Q) [τ_2 = 2.02 ms (46%)]. This indicates that binding of Tb^{3+} at EF-hand 4 induces a restructuring of the coordination sphere similar to that induced when both EF-hands 3 and 4 are bound to Tb^{3+}. On the other hand, the structural arrangement of the binding loop at EF-hand 3 when Tb^{3+} is bound at this site is significantly different, with a much more solvent-exposed Tb^{3+} ion. However, it could also be possible that these two lifetimes cannot be separately resolved in the DREAM(Δ64) decays. The lifetime of Tb^{3+} bound at the solvent-exposed site is identical on both

constructs, with τ_1 being 0.62 ms (50%) for DREAM(E186Q) and τ_1 being 0.63 ms (27%) for DREAM(E234Q), but faster than that observed for the fully active proteins. Interestingly, in the presence of 5 mM Mg^{2+}, a decrease in the decay lifetimes and an increase in the intensity contribution of the long-lived decay are observed for all constructs, except for DREAM(E234Q). The observed changes are largest for DREAM(E186Q) where a decrease of 0.44 ms in τ_2 is also accompanied by a 15% increase in the contribution of this decay component. The decay lifetimes, τ_1 = 0.74 ms for DREAM(Δ64) and τ_1 = 0.63 ms for DREAM-(Δ160), are still longer than those for Tb^{3+} in water, while those of DREAM(E186Q) and DREAM(E234Q) are identical to that of Tb^{3+} in water. The effect of Mg^{2+} on the luminescence data is in good agreement with the changes observed in the sensitized emission titrations (Figure 3d).

Finally, we examined whether Tb^{3+} luminescence decay would be sensitive to structural changes induced on CaM and DREAM upon binding of small hydrophobic ligands. To test this hypothesis, we chose trifluoperazine (TFP) and a novel biphenyl-urea compound named NS5806. These compounds have been shown to bind at hydrophobic cavities on CaM and DREAM, respectively, in a calcium-dependent manner.[20,49] Upon titration of each ligand into Tb^{3+}-bound CaM and DREAM(Δ64), we observe a strong dose-dependent modulation of the luminescence decay (Figure 6d). Global analysis of the luminescence decay of the Tb^{3+}CaM and Tb^{3+}DREAM-(Δ64) complexes reveals that binding of these small hydrophobic ligands induces a decrease in intensity contribution from τ_2 on both constructs while also decreasing the long lifetime on DREAM(Δ64). Plotting the change in f_2 as a function of TFP or NS5806 concentration yields dissociation constants of ~37 μM for both ligands (data not shown), which is larger than those observed in the Ca^{2+}-bound form of these proteins (K_d ~ 1 μM for TFP, and K_d = 5 μM for NS5806). The discrepancies could be due to secondary sites being populated (TFP has been shown to bind at four sites on CaM with dissociation constants between 1 μM and 5 mM) or to the distinct conformation of the hydrophobic cavity of the proteins in the Tb^{3+}-bound form.

Displacement of Ca^{2+} by Tb^{3+} Induces Minimal Changes in the Collisional Cross Section of DREAM

To further study the displacement of Ca^{2+} ions from the EF-hand domains of DREAM, as well as to determine the magnitude of the structural differences between the Ca^{2+}- and Tb^{3+}-bound DREAM structures, ion mobility measurements were conducted to determine the ion-neutral collisional cross section using a TIMS–MS analyzer (see Table 4). The mass spectrum of DREAM(Δ64) under native nanoESI conditions shows a narrow charge-state distribution (+7 to +9), with multiple Ca^{2+} and Tb^{3+} adducts. A closer look at the charge distribution shows the presence of the apo form, $[M + nH]^{n+}$, as well as three adduct series: $[M + Ca^{2+}_{x=1–3} + (n–x)H]^{n+}$, $[M + Ca^{2+}_{x} + Tb^{3+}_{y} + (n–x–y)H]^{n+}$, and $[M + Tb^{3+}_{x=1–2} + (n–x)H]^{n+}$ [see the example of the +8 charge-state distribution of DREAM-(Δ64) in the presence of Ca^{2+}, Ca^{2+} and Tb^{3+}, and Tb^{3+} in Figure 7a]. Inspection of the mobility profiles for each adduct series shows that as the charge state increases from +7 to +9, a decrease in mobility (and increase in CCS) is observed as a consequence of the interaction of the molecular ion with the external electric field, which is not necessarily an indication of conformational changes. However, small changes in the CCS are observed as a function of

the adduct series within each charge state. For example, a decrease in the CCS is observed for DREAM(Δ64) bound to Tb^{3+} when compared to that of DREAM(Δ64) bound to Ca^{2+} and DREAM(Δ64) bound to Ca^{2+} and Tb^{3+} (see Figure 7b). Comparison of the observed CCS profiles (CCS_{+7-+9} = 2200–2300 $Å^2$) to that of a previously reported 2JUL NMR structure of DREAM[7] (CCS_{theo} = 2773 $Å^2$) suggests that the gas-phase conformations are more compact than that observed in solution, probably as a consequence of the interaction of the adduct with the EF-hand domains in the absence of the solvent. In addition, the higher affinity of Tb^{3+} when compared to that of Ca^{2+} may induce a more compact structure (smaller CCS) for DREAM(Δ64) bound to Tb^{3+} than for DREAM(Δ64) bound to Ca^{2+} and DREAM(Δ64) bound to Ca^{2+} and Tb^{3+} in the absence of the solvent.

DISCUSSION

In this report, we present conclusive evidence that Tb^{3+} is able to bind at the C-terminus of DREAM and displace Ca^{2+} from the binding loop at EF-hands 3 and 4. Using circular dichroism as well as fluorescence intensity and anisotropy decay of intrinsic fluorescent probes, we demonstrate that Tb^{3+} is able to induce structural changes on DREAM identical to those observed upon Ca^{2+} binding. Circular dichroism shows a small deviation of the spectra near 208 nm, a region that is sensitive to the presence of antiparallel β-sheets.[50] DREAM is mainly α-helical, and the only region in which small antiparallel β-sheets are formed is between the metal binding loops of each EF-hand pair.[7] Therefore, it is possible that association of Tb^{3+} induces structural changes at the metal binding loop that result in a loss of these short β-sheet regions. Small differences between Tb^{3+}- and Ca^{2+}-bound DREAM were also observed by anisotropy decay measurements. Anisotropy decay revealed that dimers are formed in the Ca^{2+}- or Tb^{3+}-bound form of DREAM, but binding of Tb^{3+} induces a more dynamic environment near Trp169. Using molecular dynamics, we have previously shown that Trp169 in DREAM(Δ64) can populate two rotamers, and it is possible that Tb^{3+} binding could enhance this rotamer transition, which would result in an increase in local dynamics.[43]

As seen for other calcium binding proteins, we observe that aromatic amino acids at the C-terminus are able to transfer energy to the bound Tb^{3+}. Specifically, we show that mutation of Y174 to alanine results in a significant reduction (~60%) in the sensitized emission of Tb^{3+} at 545 nm, while maintaining identical 280 nm/295 nm ratios compared to that of DREAM(Δ64). Together, these results highlight the presence of an antenna effect, in which W169 is the main donor to Tb^{3+}. Attempts to use sensitized emission and Tb^{3+} titrations to elucidate the lanthanide binding sequence to EF-hands 3 and 4 on DREAM indicate that both EF-hands bind Tb^{3+} with a similar affinity [K_d = 5.9 μM for DREAM(E234Q), and K_d = 11 μM for DREAM(E186Q)]. Because these experiments were conducted in the presence of excess calcium and magnesium, inactivation of each EF-hand actually favors binding to the mutated loop (see ITC results). Therefore, we are unable to identify whether the slightly lower affinity of Tb^{3+} with the DREAM(E186Q) mutant is due to the inherent lower affinity to this hand or because a metal ion (Ca^{2+} or Mg^{2+}) is loosely bound at this mutated site. Nonetheless, one of the most salient observations of these Tb^{3+} titration experiments is that in the presence of Mg^{2+}, the sensitized emission of Tb^{3+} decreases by more than 50%. This decrease in intensity at 545 nm could be due to either Mg^{2+}-induced structural

rearrangements of the environment near Trp169 or rearrangement of the Tb^{3+} binding loop at EF-hands 3 and 4. Indeed, we observe that EF-hand 3, which is next to EF-hand 2, is more sensitive to magnesium binding. These results support the idea that Mg^{2+} plays a structural role in DREAM and that at physiological concentrations it may act as a functional cofactor through interaction with EF-hand 2.

Isothermal calorimetry experiments show that Tb^{3+} displacement of Ca^{2+} from EF-hands 3 and 4 on DREAM(Δ64) in the presence of 5 mM Mg^{2+} is associated with a ΔG of −14 kcal mol^{-1}, while the displacement energy for the DREAM(Δ160) construct is −12 kcal mol^{-1}. The same displacement process for EF-hands 1–4 in CaM is associated with a free energy ΔG of −18 kcal mol^{-1}. The more favorable displacement of Ca^{2+} from CaM EF-hands compared to DREAM(Δ64) highlights the stronger association of Ca^{2+} in the latter.[42] Throughout this report, we correlate the K_1 thermodynamic parameters with displacement of Ca^{2+} from EF-hand 3 and K_2 with displacement from EF-hand 4 in the DREAM(Δ64), DREAM(E186Q), and DREAM(E234Q) constructs. Even though these correlations are not unequivocally proven by our results, they are supported by the associated changes in enthalpy and entropy under different conditions. Following this assignment, we can approximate the enthalpy and entropy associated with coordination of Tb^{3+} by Glu at position 12 of EF-hands 3 and 4 by calculating $\Delta H_{Glu}^{(Mutant)} = \Delta H_i^{DREAM(\Delta 64)} - \Delta H_i^{DREAM(Mutant)}$ and $T\Delta S_{Glu}^{(Mutant)} = T\Delta S_i^{DREAM(\Delta 64)} - T\Delta S_i^{DREAM(Mutant)}$, where the subscript i is 1 for DREAM-(E186Q) and 2 for DREAM(E234Q). These calculations reveal that coordination of Tb^{3+} by Glu186 of EF-hand 3 is associated with a $\Delta H_{Glu}^{(E186Q)}$ of 4.5 kcal mol^{-1} and a $T\Delta S_{Glu}^{(E186Q)}$ of 5.0 kcal mol^{-1}. In contrast, Glu234 of EF-hand 4 has a 3-fold larger enthalpy and entropy contribution, with a $\Delta H_{Glu}^{(E234Q)}$ of 14 kcal mol^{-1} and a $T\Delta S_{Glu}^{(E234Q)}$ of 15 kcal mol^{-1}. In both cases, coordination of the metal ion is driven by favorable entropy contributions, likely due to release of a water molecule upon coordination of Glu at position 12. These results are similar to those observed for Ca^{2+} binding to CaM and DREAM(Δ64) in which entropy was observed to be the main driving force.[42,44] In contrast, the enthalpic contribution due to metal binding to the EF-hands of CaM and DREAM(Δ64) has been shown to be very small. It is possible that the unfavorable endothermic process observed here is due to additional structural changes associated with Glu12 coordination. The larger enthalpy and entropy associated with coordination of Glu12 on EF-hand 4 highlights the role of this EF-hand in controlling the activation of DREAM. Indeed, Glu12 is positioned on the exiting helix of EF-hand 4 that is immediately adjacent to a hydrophobic cavity that mediates the calcium-regulated co-assembly with potassium channels and small ligands.[20,51,52]

Another interesting aspect of the recovered thermodynamic parameters shown in Table 2 is that the enthalpy and entropy recovered for all the titrations are highly correlated. This correlation has been observed before for Ca^{2+} binding to CaM[44] as well as in other systems.[53] More importantly, the linear relationship of $T\Delta S$ as a function of ΔH allows us to extrapolate the entropy associated with displacement of Ca^{2+}, prior to any structural change induced by Tb^{3+} (Figure 8). This is based on the idea that displacement of Ca^{2+} by Tb^{3+} is not associated with the formation or breakage of any new bond because the coordinations of Ca^{2+} and Tb^{3+} in bulk water are identical. Extrapolating the linear relationship yields a $T\Delta S_{displacement}$ value of 6.9 ± 0.2 kcal mol^{-1}, which is similar to the value obtained for

binding of Ca^{2+} to metal-free CaM in which $T\Delta S_{bind} = 7.2 \pm 0.1$ kcal mol^{-1}.[44] A possible explanation for the entropic gain could be due to an increase in the dynamics of the protein, something that is supported by the anisotropy decay data. The correlation of enthalpy and entropy can also be explained by a process that involves the release of water following the association of two ions of opposite charges in solution. The resulting charge neutralization would facilitate the mobilization of solvent molecules from the surface of the protein into the bulk water.[54] This release of water molecules is associated with an unfavorable endothermic process (breakage of water–protein hydrogen bonds) and favorable positive change in entropy. Indeed, Ca^{2+}-bound DREAM(Δ64) (net charge of −3 at pH 7.4) and Ca^{2+}-bound CaM (net charge of −16 at pH 7.4) would be neutralized by 2 and 8 units upon Tb^{3+} displacement, respectively. This charge neutralization effect could also partially account for the decreased enthalpy and entropy contribution of the DREAM(E186Q) and DREAM(E234Q) mutants, both of which have one less negative charge than DREAM(Δ64) does.

Sensitized emission, circular dichroism, TIMS–MS, and ITC experiments provide information about global structural changes of the protein upon displacement of Ca^{2+} by Tb^{3+}. On the other hand, luminescence studies allow us to gain better insight into the immediate coordination sphere of Tb^{3+} ion, and how this environment is affected by inactivation of EF-hands, Mg^{2+} binding, ionic strength, and/or ligand binding. Measurements of the luminescence decay of Tb^{3+} bound to different constructs highlight the idea that Tb^{3+} bound at EF-hand 3 is more solvent-exposed than Tb^{3+} bound at EF-hand 4. Nonetheless, the decay observed for DREAM(Δ64) is much slower than that observed for CaM, indicating that the coordination around Tb^{3+} in DREAM greatly restricts the accessibility of water. We also observe that the luminescence decays are widely affected by addition of excess Mg^{2+}, supporting the idea that some secondary sites of Tb^{3+} binding, including EF-hand 2 on DREAM, are identical to those of Mg^{2+} binding. The high sensitivity of EF-hand 3 to Mg^{2+} binding could also be due to propagated rearrangement of EF-hand 2 upon association of Mg^{2+}. It is also possible that binding of Mg^{2+} at these secondary sites is responsible for the observed rearrangement of the EF-hand loops. The overall picture that emerges from these observations is that Mg^{2+} is able to modulate the protein structure and that secondary metal sites may play a role in modulating protein conformation. Indeed, previous work and our unpublished results support the idea that two Ca^{2+} specific sites and additional secondary sites are found on DREAM(Δ160).[10] Lastly, titration of small hydrophobic ligands also reveals that the environment near the metal binding loops of EF-hands 3 and 4 is sensitive to association of ligand with DREAM. Altogether, these observations highlight the idea that association of these small molecules at the hydrophobic surfaces of CaM and DREAM induces conformational changes that not only can distort the coordination geometry of Tb^{3+} at the binding loops but also could potentially facilitate dissociation of Tb^{3+} from the protein.

Finally, ion mobility and mass spectrometry measurements support the hypothesis that Tb^{3+} can displace Ca^{2+} from EF-hands 3 and 4 and that the resulting folded conformation of the Tb^{3+}-bound DREAM(Δ64) protein is almost identical to that of the calcium-bound protein during native ESI conditions. Comparison of the observed CCS profiles to that of a previously reported NMR structure of DREAM[7] suggested that the gas-phase conformations

are more compact than that observed in solution, probably as a consequence of the interaction of the adduct with the EF-hand domains in the absence of the solvent. In addition, the higher affinity of Tb^{3+} when compared to that of Ca resulted in more compact structures (smaller CCS) for DREAM(Δ64) bound to Tb^{3+} than for DREAM(Δ64) bound to Ca^{2+} and DREAM(Δ64) bound to Ca^{2+} and Tb^{3+} in the absence of the solvent.

CONCLUSION

In this report, we show compelling evidence supporting the specific association of Tb^{3+} with EF-hands 3 and 4 of DREAM. We also demonstrate that replacement of Ca^{2+} with Tb^{3+} leads to an increase in the dynamics of the protein; however, the structural and functional properties between DREAM bound to either metal are highly similar. We show that like the case for CaM, Tb^{3+} bound to DREAM can be sensitized by aromatic amino acids at the C-terminus, with tryptophan 169 being the main energy donor. The high affinity of the EF-hands for Tb^{3+} and the fluorescence properties of this lanthanide have allowed us to highlight the role of Mg^{2+} as a structural cofactor, which can bind to EF-hand 2 and modify the immediate environment near the calcium binding loops of EF-hands 3 and 4. Isothermal calorimetry also highlights the role of EF-hand 4 in mediating calcium-regulated ligand recognition in DREAM. These findings provide structural information about DREAM and will facilitate future structural NMR studies and lanthanide resonance energy transfer experiments aimed at exploring the association of DREAM with other proteins.

Supplementary Material

Refer to Web version on PubMed Central for supplementary material.

Acknowledgments

Funding

This work was supported by the National Science Foundation (MCB 1021831, J.M.) and the National Institutes of Health (Grant R00GM106414, F.F.-L.). W.G.G. was fully supported by National Institute of General Medical Sciences Grant R25 GM061347.

ABBREVIATIONS

DREAM	downstream regulatory element antagonist modulator
CaM	calmodulin
fwhm	full width at half-maximum
KChIP	potassium channel-interacting protein
DREAM(Δ64)	mouse DREAM construct lacking residues 1–64
1,8-ANS	8-anilinonaphthalene-1-sulfonic acid
CD	circular dichroism
TIMS–MS	trapped ion mobility spectrometry–mass spectrometry

TFP	trifluoperazine

References

1. Carrion AM, Link WA, Ledo F, Mellstrom B, Naranjo JR. DREAM is a Ca2+-regulated transcriptional repressor. Nature. 1999; 398:80–84. [PubMed: 10078534]
2. Buxbaum JD, Choi E, Luo Y, Lilliehook C, Crowley AC, Merriam DE, Wasco W. Calsenilin: A calcium-binding protein that interacts with the presenilins and regulates the levels of a presenilin fragment. Nat Med. 1998; 4:1177–1181. [PubMed: 9771752]
3. An WF, Bowlby MR, Betty M, Cao J, Ling H, Mendoza G, Hinson JW, Mattsson KI, Strassle BW, Trimmer JS, Rhodes KJ. Modulation of A-type potassium channels by a family of calcium sensors. Nature. 2000; 403:553–556. [PubMed: 10676964]
4. Cheng HM, Pitcher GM, Laviolette SR, Whishaw IQ, Tong KI, Kockeritz LK, Wada T, Joza NA, Crackower M, Goncalves J, Sarosi I, Woodgett JR, Oliveira-dos-Santos AJ, Ikura M, van der Kooy D, Salter MW, Penninger JM. DREAM is a critical transcriptional repressor for pain modulation. Cell. 2002; 108:31–43. [PubMed: 11792319]
5. Costigan M, Woolf CJ. No DREAM, no pain: Closing the spinal gate. Cell. 2002; 108:297–300. [PubMed: 11853663]
6. Fontán-Lozano Á, Romero-Granados R, del-Pozo-Martín Y, Suárez-Pereira I, Delgado-García JM, Penninger JM, Carrión ÁM. Lack of DREAM protein enhances learning and memory and slows brain aging. Curr Biol. 2009; 19:54–60. [PubMed: 19110430]
7. Lusin JD, Vanarotti M, Li C, Valiveti A, Ames JB. NMR structure of DREAM: Implications for Ca2+-dependent DNA binding and protein dimerization. Biochemistry. 2008; 47:2252–2264. [PubMed: 18201103]
8. da Silva AC, Kendrick-Jones J, Reinach FC. Determinants of ion specificity on EF-hands sites. conversion of the Ca2+/Mg2+ site of smooth muscle myosin regulatory light chain into a ca(2+)-specific site. J Biol Chem. 1995; 270:6773–6778. [PubMed: 7896823]
9. Gifford J, Walsh M, Vogel H. Structures and metalion-binding properties of the Ca2 -binding helix-loop-helix EF-hand motifs. Biochem J. 2007; 405:199–221. [PubMed: 17590154]
10. Craig TA, Benson LM, Venyaminov SY, Klimtchuk ES, Bajzer Z, Prendergast FG, Naylor S, Kumar R. The metal-binding properties of DREAM. J Biol Chem. 2002; 277:10955–10966. [PubMed: 11788589]
11. Kretsinger RH, Nockolds CE. Carp muscle calcium-binding protein. II structure determination and general description. J Biol Chem. 1973; 248:3313–3326. [PubMed: 4700463]
12. Osawa M, Tong KI, Lilliehook C, Wasco W, Buxbaum JD, Cheng HYM, Penninger JM, Ikura M, Ames JB. Calcium-regulated DNA binding and oligomerization of the neuronal calcium-sensing protein, Calsenilin/DREAM/KChIP3. J Biol Chem. 2001; 276:41005–41013. [PubMed: 11535596]
13. Gonzalez WG, Miksovska J. Application of ANS fluorescent probes to identify hydrophobic sites on the surface of DREAM. Biochim Biophys Acta, Proteins Proteomics. 2014; 1844:1472–1480.
14. Mustafi SM, Mukherjee S, Chary KVR, Del Bianco C, Luchinat C. Energetics and mechanism of Ca2+ displacement by lanthanides in a calcium binding protein. Biochemistry. 2004; 43:9320–9331. [PubMed: 15260475]
15. Martin B, Richardson FS. Lanthanides as probes for calcium in biological systems. Q Rev Biophys. 1979; 12:181–209. [PubMed: 386412]
16. Rao ST, Satyshur KA, Greaser ML, Sundaralingam M. X-ray structures of mn, cd and tb metal complexes of troponin C. Acta Crystallogr Sect D: Biol Crystallogr. 1996; 52:916–922. [PubMed: 15299599]
17. Pintacuda G, Park AY, Keniry MA, Dixon NE, Otting G. Lanthanide labeling offers fast NMR approach to 3D structure determinations of Protein-Protein complexes. J Am Chem Soc. 2006; 128:3696–3702. [PubMed: 16536542]

18. Gonzalez W, Miksovska J. Characterization of the photophysical, thermodynamic and structural properties of the terbium (III)-KChIP3 complex. Biophys J. 2015; 108:218a.
19. Gonzalez WG, Arango AS, Miksovska J. Amphiphilic residues 29–44 of DREAM N-termini mediate calmodulin:DREAM complex formation. Biochemistry. 2015; 54:4391–4403. [PubMed: 26108881]
20. Gonzalez WG, Pham K, Miksovska J. Modulation of the voltage-gated potassium channel (Kv4.3) and the auxiliary protein (KChIP3) interactions by the current activator NS5806. J Biol Chem. 2014; 289:32201–32213. [PubMed: 25228688]
21. George SE, Su Z, Fan D, Means AR. Calmodulin-cardiac troponin C chimeras. effects of domain exchange on calcium binding and enzyme activation. J Biol Chem. 1993; 268:25213–25220. [PubMed: 8227086]
22. Fernandez-Lima F, Kaplan D, Park M. Note: Integration of trapped ion mobility spectrometry with mass spectrometry. Rev Sci Instrum. 2011; 82:126106. [PubMed: 22225261]
23. Fernandez-Lima F, Kaplan DA, Suetering J, Park MA. Gas-phase separation using a trapped ion mobility spectrometer. Int J Ion Mobility Spectrom. 2011; 14:93–98.
24. Molano-Arevalo JC, Hernandez DR, Gonzalez WG, Miksovska J, Ridgeway ME, Park MA, Fernandez-Lima F. Flavin adenine dinucleotide structural motifs: From solution to gas phase. Anal Chem. 2014; 86:10223–10230. [PubMed: 25222439]
25. Hernandez DR, DeBord JD, Ridgeway ME, Kaplan DA, Park MA, Fernandez-Lima F. Ion dynamics in a trapped ion mobility spectrometer. Analyst. 2014; 139:1913–1921. [PubMed: 24571000]
26. McDaniel, EW.; Mason, EA. The Mobility and Diffusion of Ions in Gases. Wiley; New York: 1973.
27. Larriba C, Hogan CJ Jr. Ion mobilities in diatomic gases: Measurement versus prediction with non-specular scattering models. J Phys Chem A. 2013; 117:3887–3901. [PubMed: 23488939]
28. Larriba C, Hogan CJ. Free molecular collision cross section calculation methods for nanoparticles and complex ions with energy accommodation. J Comput Phys. 2013; 251:344–363.
29. Ouyang H, Larriba-Andaluz C, Oberreit DR, Hogan CJ Jr. The collision cross sections of iodide salt cluster ions in air via differential mobility analysis-mass spectrometry. J Am Soc Mass Spectrom. 2013; 24:1833–1847. [PubMed: 24026975]
30. Mulqueen P, Tingey JM, Horrocks WD. Characterization of lanthanide(III) ion binding to calmodulin using luminescence spectroscopy. Biochemistry. 1985; 24:6639–6645. [PubMed: 4084548]
31. Chaudhuri D, Horrocks WD Jr, Amburgey JC, Weber DJ. Characterization of lanthanide ion binding to the EF-hand protein S100 beta by luminescence spectroscopy. Biochemistry. 1997; 36:9674–9680. [PubMed: 9245399]
32. Kilhoffer M, Gerard D, Demaille JG. Terbium binding to octopus calmodulin provides the complete sequence of ion binding. FEBS Lett. 1980; 120:99–103. [PubMed: 7439394]
33. Austin RH, Stein DL, Wang J. Terbium luminescence-lifetime heterogeneity and protein equilibrium conformational dynamics. Proc Natl Acad Sci U S A. 1987; 84:1541–1545. [PubMed: 3470740]
34. Horrocks WD, Sudnick DR. Lanthanide ion probes of structure in biology. laser-induced luminescence decay constants provide a direct measure of the number of metal-coordinated water molecules. J Am Chem Soc. 1979; 101:334–340.
35. Hagan AK, Zuchner T. Lanthanide-based time-resolved luminescence immunoassays. Anal Bioanal Chem. 2011; 400:2847–2864. [PubMed: 21556751]
36. Fisher JR, Sharma Y, Iuliano S, Piccioti RA, Krylov D, Hurley J, Roder J, Jeromin A. Purification of myristoylated and nonmyristoylated neuronal calcium sensor-1 using single-step hydrophobic interaction chromatography. Protein Expression Purif. 2000; 20:66–72.
37. Drabikowski W, Brzeska H, Venyaminov SYu. Tryptic fragments of calmodulin. Ca2+- and Mg2+-induced conformational changes. J Biol Chem. 1982; 257:11584–11590. [PubMed: 6811583]
38. Hogue CW, MacManus JP, Banville D, Szabo AG. Comparison of terbium (III) luminescence enhancement in mutants of EF hand calcium binding proteins. J Biol Chem. 1992; 267:13340–13347. [PubMed: 1618836]

39. Brittain HG, Richardson FS, Martin RB. Terbium(III) emission as a probe of calcium(II) binding sites in proteins. J Am Chem Soc. 1976; 98:8255–8260. [PubMed: 993525]
40. Kleinerman M. Energy migration in lanthanide chelates. J Chem Phys. 1969; 51:2370–2381.
41. Wallace RW, Tallant EA, Dockter ME, Cheung WY. Calcium binding domains of calmodulin. sequence of fill as determined with terbium luminescence. J Biol Chem. 1982; 257:1845–1854. [PubMed: 6276400]
42. Osawa M, Dace A, Tong KI, Valiveti A, Ikura M, Ames JB. Mg2+ and Ca2+ differentially regulate DNA binding and dimerization of DREAM. J Biol Chem. 2005; 280:18008–18014. [PubMed: 15746104]
43. Pham K, Dhulipala G, Gonzalez WG, Gerstman BS, Regmi C, Chapagain PP, Miksovska J. Ca2+ and Mg2+ modulate conformational dynamics and stability of downstream regulatory element antagonist modulator. Protein Sci. 2015; 24:741–751. [PubMed: 25627705]
44. Gilli R, Lafitte D, Lopez C, Kilhoffer M, Makarov A, Briand C, Haiech J. Thermodynamic analysis of calcium and magnesium binding to calmodulin. Biochemistry. 1998; 37:5450–5456. [PubMed: 9548926]
45. Wang CL, Aquaron RR, Leavis PC, Gergely J. Metal-binding properties of calmodulin. Eur J Biochem. 1982; 124:7–12. [PubMed: 7084230]
46. Hungerford G, Hussain F, Patzke GR, Green M. The photophysics of europium and terbium polyoxometalates and their interaction with serum albumin: A time-resolved luminescence study. Phys Chem Chem Phys. 2010; 12:7266–7275. [PubMed: 20490399]
47. Bünzli, JCG.; Eliseeva, SV. Lanthanide Luminescence. Springer; Berlin: 2011. Basics of lanthanide photophysics; p. 1-45.
48. Deiters E, Song B, Chauvin A, Vandevyver C, Gumy F, Bünzli J. Luminescent bimetallic lanthanide bioprobes for cellular imaging with excitation in the visible-light range. Chem – Eur J. 2009; 15:885–900. [PubMed: 19065695]
49. Cook WJ, Walter LJ, Walter MR. Drug binding by calmodulin: Crystal structure of a calmodulin-trifluoperazine complex. Biochemistry. 1994; 33:15259–15265. [PubMed: 7803388]
50. Kelly SM, Jess TJ, Price NC. How to study proteins by circular dichroism. Biochim Biophys Acta, Proteins Proteomics. 2005; 1751:119–139.
51. Wang H, Yan Y, Liu Q, Huang Y, Shen Y, Chen L, Chen Y, Yang Q, Hao Q, Wang K, Chai J. Structural basis for modulation of Kv4 K+ channels by auxiliary KChIP subunits. Nat Neurosci. 2007; 10:32–39. [PubMed: 17187064]
52. Pioletti M, Findeisen F, Hura GL, Minor DL. Three-dimensional structure of the KChIP1-Kv4.3 T1 complex reveals a cross-shaped octamer. Nat Struct Mol Biol. 2006; 13:987–995. [PubMed: 17057713]
53. Kuroki R, Yutani K. Structural and thermodynamic responses of mutations at a Ca2+ binding site engineered into human lysozyme. J Biol Chem. 1998; 273:34310–34315. [PubMed: 9852096]
54. Bowman-James, K.; Bianchi, A.; García-Espana, E. Anion Coordination Chemistry. John Wiley & Sons; New York: 2012.

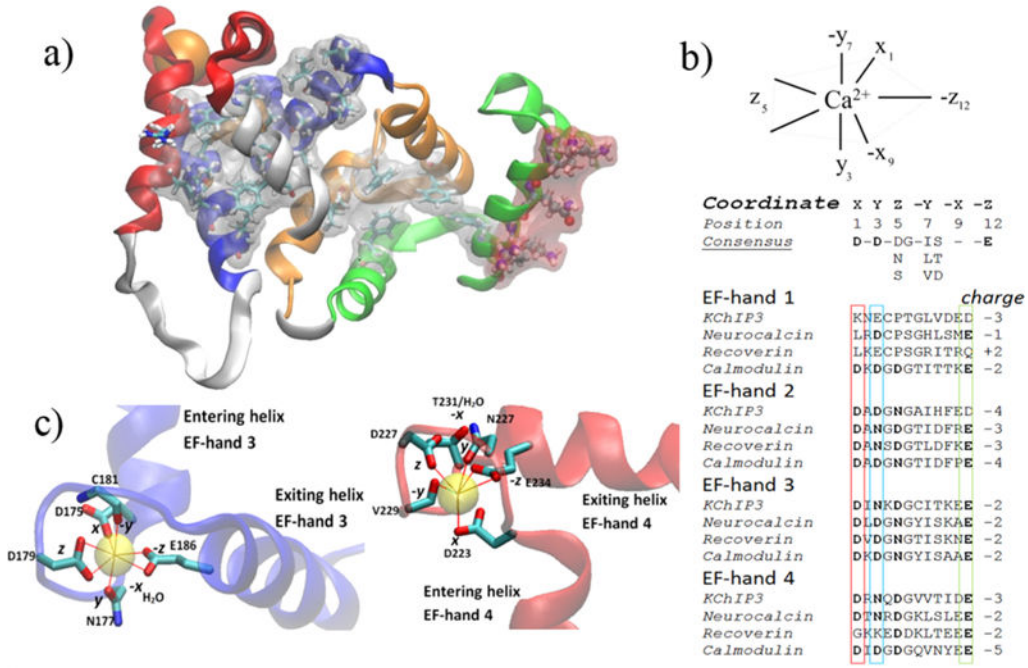

Figure 1.

(a) NMR structure of DREAM monomer with highlighted hydrophobic residues (gray mesh) and charged residues (red mesh) (Protein Data Bank entry 2JUL).[7] The four EF-hands of DREAM are colored green (EF-hand 1), orange (EF-hand 2), blue (EF-hand 3), and red (EF-hand 4). Calcium is shown as an orange sphere. (b) Coordination geometry of calcium bound to EF-hand 3 (left) and EF-hand 4 (right). Residues involved in coordination of Ca^{2+} are shown as a licorice model. EF-hand 3 shows a clear pentagonal bipyramidal coordination, whereas EF-hand 4 is distorted. (c) Geometry and consensus sequence of EF-hand binding loops as well as sequence homology between neuronal calcium sensors and calmodulin at the metal binding loops.

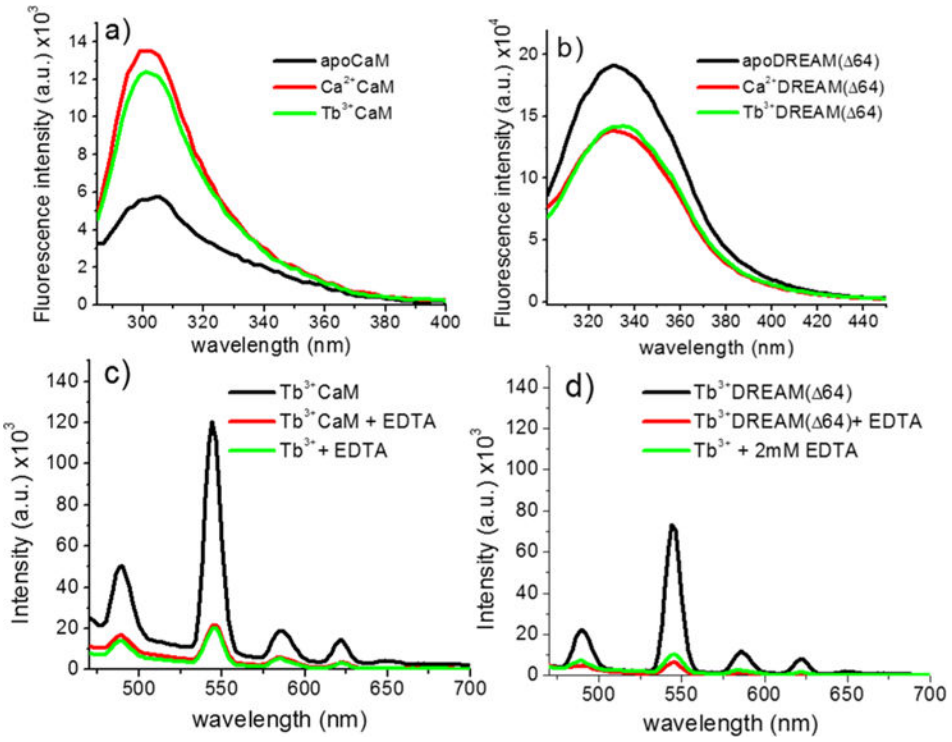

Figure 2.

Intrinsic fluorescence changes of 40 μM (a) CaM and (b) DREAM(Δ64) upon binding of 1 mM calcium or 160 μM Tb^{3+} on CaM or 80 μM Tb^{3+} for DREAM(Δ64), excited at 280 ± 4 nm. The observed tyrosine fluorescence change upon binding of Tb^{3+} to CaM shows a small deviation from that observed for Ca^{2+}, likely due to quenching of the fluorescence by energy transfer to Tb^{3+}. The Tb^{3+}-induced transition for DREAM(Δ64) is identical to that observed in the presence of Ca^{2+}. Sensitized emission of (c) 160 μM Tb^{3+} bound to CaM and (d) 80 μM Tb^{3+} bound to DREAM(Δ64), excited at 280 nm with and without 2 mM EDTA. The background emission of the Tb^{3+}:EDTA complex is shown as a reference. The observed sensitized emission of Tb^{3+} shows the characteristic sharp bands at 489, 544 (major), 586, and 622 nm due to the $^5D_4 \rightarrow {}^7F_6$, $^5D_4 \rightarrow {}^7F_5$, $^5D_4 \rightarrow {}^7F_4$, and $^5D_4 \rightarrow {}^7F_3$ transitions of Tb^{3+}, respectively. The major peak at 545 nm for DREAM(Δ64) is 40% smaller than that observed for CaM. Addition of 2 mM EDTA to either CaM or DREAM(Δ64) resulted in an emission identical to that of Tb^{3+} in solution.

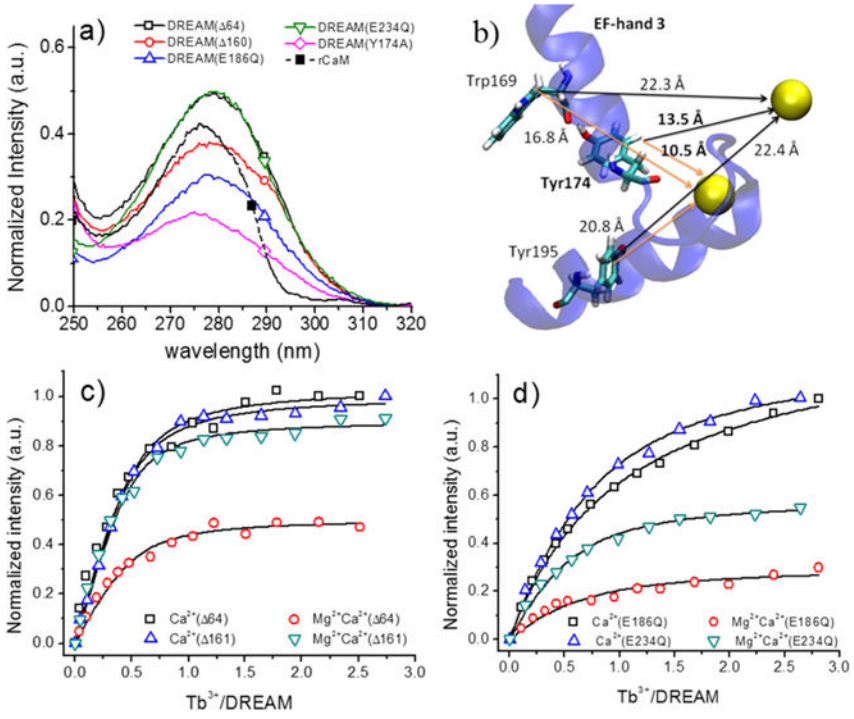

Figure 3.

(a) Excitation spectra of DREAM constructs bound to Tb^{3+} (20 μM protein with 40 μM Tb^{3+}). The spectra were normalized so that the intensity corresponding to backbone to Tb^{3+} energy transfer at 240 nm is the same for DREAM(Δ64), DREAM(Δ160), and DREAM(Y174A) while the magnitude is half for DREAM(E186Q) and DREAM(E234Q). (b) Calcium/terbium binding sites of EF-hands 3 and 4. Only EF-hand 3 is shown (blue) for the sake of clarity. (c) Titrations of Tb^{3+} into DREAM(Δ64) and DREAM(Δ160) in 20 mM TRIS (pH 7.4) and 100 μM Ca^{2+} with and without 5 mM Mg^{2+}. (d) Titration of Tb^{3+} into DREAM(E186Q) and DREAM(E234Q) under the conditions described for panel c. Solid lines represent the best fit using the quadratic equation for *N* binding sites.

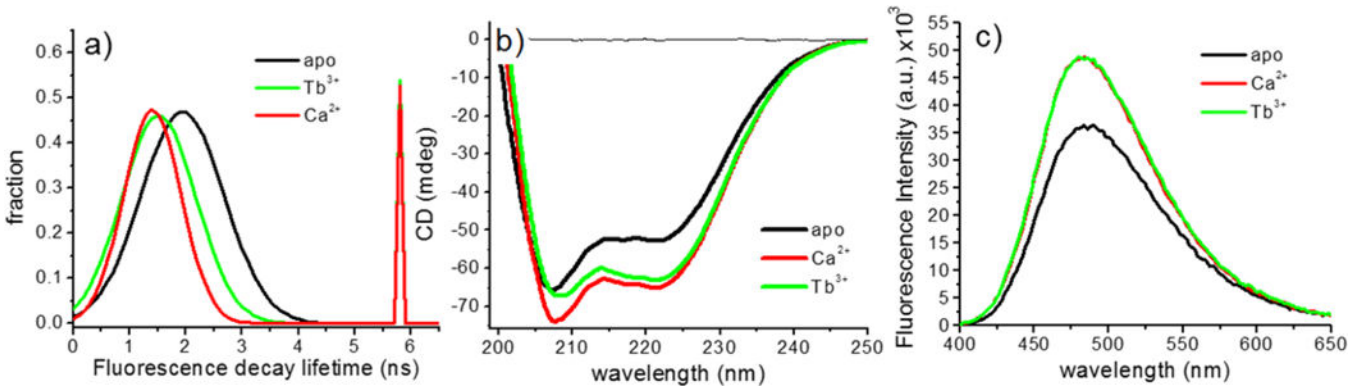

Figure 4.

(a) Tryptophan fluorescence lifetime distribution of DREAM(Δ64) in the presence of Ca^{2+} or Tb^{3+}. Decay data were modeled as a Gaussian distribution and a discrete decay (parameters listed in Table 1). (b) Circular dichroism spectra of 40 μM DREAM(Δ64) in the presence of 1 mM Ca^{2+}, 2 mM EDTA, or 160 μM Tb^{3+} in 5 mM TRIS (pH 7.4). (c) Binding of Tb^{3+} or Ca^{2+} to 10 μM DREAM(Δ64) in the presence of 40 μM 1,8-ANS.

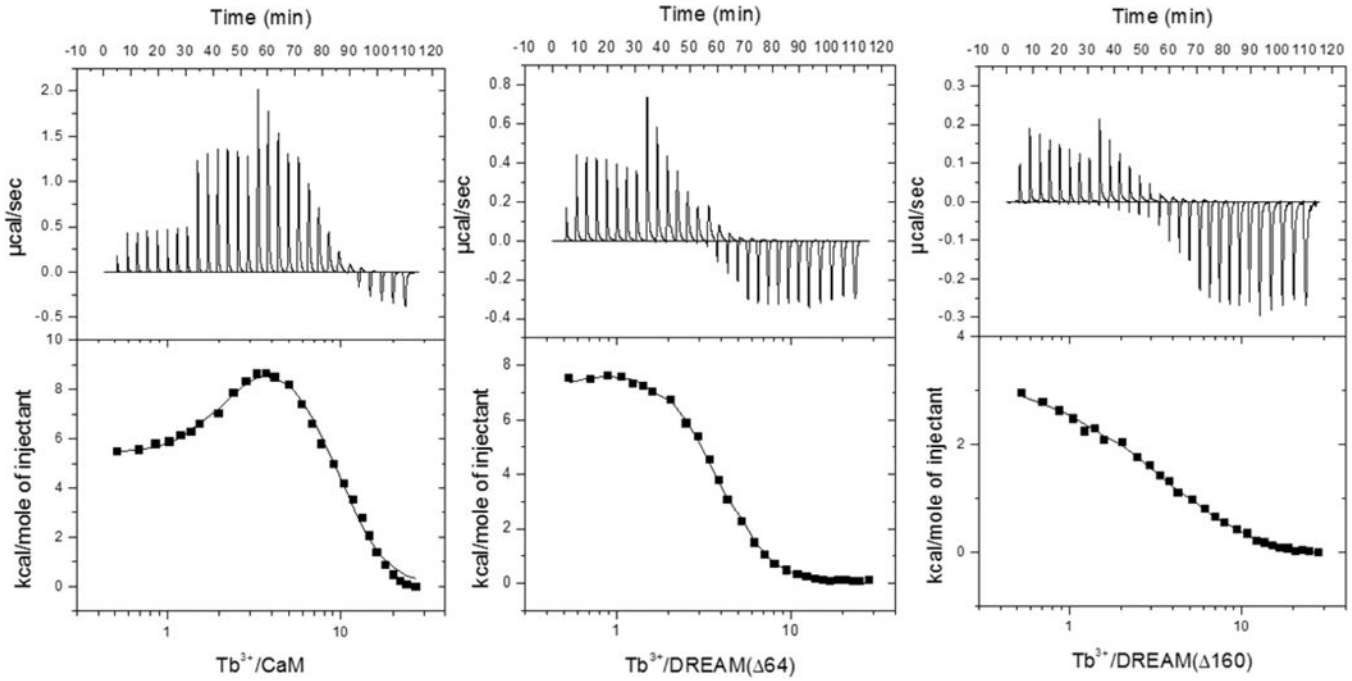

Figure 5.

ITC isotherms for Tb^{3+} displacement of Ca^{2+} from CaM, DREAM(Δ64), and DREAM(Δ160). The top panels of each profile reflect the thermal power expressed in units of microcalories per second. The bottom panels show integrated reaction heats (ΔH) expressed in units of kilocalories per mole. The solid lines present the best fitting curve with the parameters listed in Table 2.

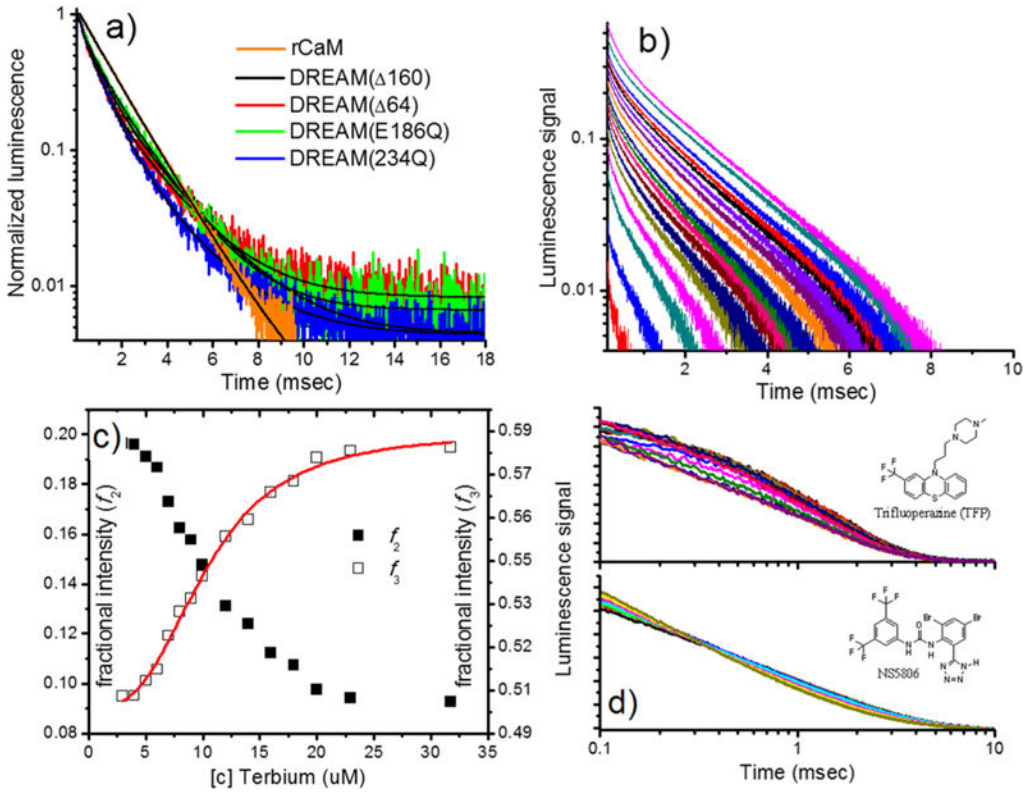

Figure 6.

(a) Luminescence decay of Tb^{3+} bound to CaM and constructs of DREAM, with 4:1 Tb^{3+}:CaM and 2:1 Tb^{3+}:DREAM stoichiometric ratios. Solid lines represent the best fit using Globals software analysis, and recovered parameters listed in Table 3. (b) Luminescence intensity decay profiles as a function of Tb^{3+} binding to 10 μM DREAM(Δ64). The luminescence decays in panel b were analyzed using a triple discrete model, and the fractional intensity contribution of the two slowest lifetimes is shown in c. The fastest decay component had a lifetime of ~80 μs with a <10% contribution and is not shown. (d) Luminescence decay of Tb^{3+} bound to CaM and DREAM(Δ64) as a function of the hydrophobic molecules TFP (top) bound to CaM and NS5806 (bottom) bound to DREAM(Δ64).

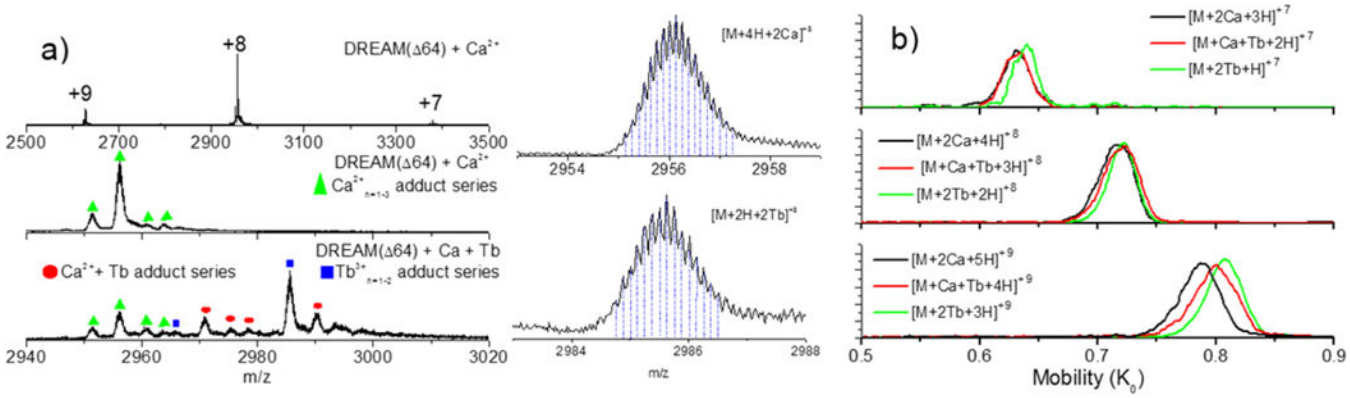

Figure 7.

(a) Typical nanoESI mass spectra of DREAM(Δ64) in the presence of Ca^{2+} and DREAM(Δ64) in the presence of Ca^{2+} and Tb^{3+}. The isotopic distributions of the DREAM(Δ64):2Ca^{2+} and DREAM(Δ64):2Tb^{3+} complexes are shown for the sake of clarity. (b) NanoESI TIMS mobility spectra of DREAM(Δ64) bound to Ca^{2+} and/or Tb^{3+}.

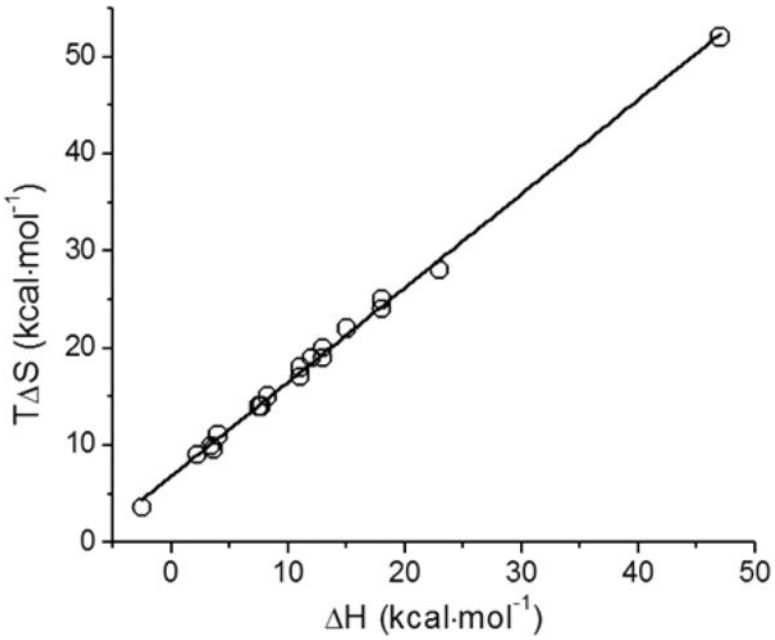

Figure 8.

Plot of $T\Delta S$ vs ΔH for Tb^{3+} displacement of Ca^{2+} from DREAM(Δ64), DREAM(Δ161), DREAM(E186Q), DREAM(E234Q), and CaM. The solid line represents the best linear fit to the data.

Table 1

Fluorescence and Anisotropy Decay Parameters of DREAM(Δ64) Bound to Ca^{2+} or Tb^{3+}[a]

	$\overline{\tau}_1$ (f_1) (ns)	w_1 (ns)	τ_2 (f_2) (ns)	$\langle\tau\rangle$ (ns)	Θ_1 (f_1) (ns)	Θ_2 (f_2) (ns)	χ^2
apoDREAM(Δ64)	1.8 (0.39)	0.69	5.7 (0.61)	4.2	0.40 (0.35)	15 (0.65)	0.5
Ca^{2+}DREAM(Δ64)	1.5 (0.48)	0.60	5.9 (0.52)	3.8	0.52 (0.40)	29 (0.60)	0.9
Tb^{3+}DREAM(Δ64)	1.5 (0.47)	0.64	5.8 (0.53)	3.8	0.23 (0.58)	27 (0.42)	1.5

[a]Values in parentheses represent the fraction intensity and fractional depolarization. τ_1 is the mean decay time of the Gaussian distribution with a width of distribution w_1. The lifetime of the discrete single-exponential term is denoted as τ_2. The average lifetime, $\langle\tau\rangle$, was calculated using eqs 1 and 2 of the Supporting Information. a_1 and a_2 are normalized pre-exponential decay fractions and f_1 and f_2 exponential decay fractions.

Table 2

ITC Parameters Recovered for Tb^{3+} Displacement of Ca^{2+} from EF-Hands of CaM and DREAM Using a Sequential Model[a]

	$K_1 \times 10^4$	$K_2 \times 10^4$	$K_3 \times 10^4$	ΔH_1	ΔH_2	ΔH_3	$T\Delta S_1$	$T\Delta S_2$	$T\Delta S_3$
CaM	29 ± 4.2	0.7 ± 0.4	5.1 ± 8.4	12 ± 5	212 ± 38	−307 ± 127	19 ± 3.9	217	−302
CaM with Mg^{2+}	8.9 ± 1.8	1.9 ± 0.2	1.4 ± 0.2	13 ± 1.5	47 ± 0.6	23 ± 7	20 ± 1.4	52 ± 0.6	28 ± 7
DREAM(Δ64)	22 ± 1.3	8.1 ± 1.6	2.8 ± 0.2	13 ± 9.0	18 ± 0.6	−2.5 ± 2.7	20 ± 9.1	24 ± 0.4	3.6 ± 2.7
DREAM(Δ64) with Mg^{2+}	16 ± 2.5	11 ± 1.1	6.0 ± 0.5	12 ± 1.3	18 ± 6.0	3.4 ± 3.2	19 ± 1.3	25 ± 5.9	9.9 ± 3.1
DREAM (Δ160)	6.9 ± 3.2	8.9 ± 9.2		13 ± 1.7	8.2 ± 1.3		19 ± 1.5	15 ± 1.1	
DREAM (Δ160) with Mg^{2+}	6.8 ± 1.4	1.8 ± 0.6		11 ± 2.2	7.7 ± 2.4		17 ± 2.1	14 ± 2.4	
DREAM (E186Q) with Mg^{2+}	14.0 ± 0.9	8.6 ± 1.3	8.8 ± 2.2	7.5 ± 1.2	15 ± 1.7	2.2 ± 2.6	14 ± 0.8	22 ± 1.8	9 ± 2.7
DREAM (E234Q) with Mg^{2+}	5.7 ± 0.9	27 ± 1.5	16 ± 6.2	11 ± 1.9	3.6 ± 2.7	4.0 ± 1.3	18 ± 1.9	9.6 ± 2.5	11 ± 0.9

[a]All experiments were conducted in triplicate at 25 °C; errors are standard deviations. Enthalpy and entropy changes shown in units of kilocalories per mole; association constants in units of inverse molar.

Table 3

Terbium(III) Luminescence Decay Parameters Recovered upon Binding to DREAM and DREAM Constructs[a]

	τ_1 (ms)	f_1	τ_2 (ms)	f_2
CaM	1.38	1.00		
CaM with TFP[b]	0.46	0.31	1.36	0.69
DREAM(Δ64)	0.86	0.59	2.22	0.14
DREAM(Δ64) with Mg^{2+}	0.74	0.54	2.05	0.24
DREAM(Δ64)*(a)*[c]	0.58	0.27	2.00	0.69
DREAM(Δ64)*(b)*[c]	0.46	0.17	2.04	0.77
DREAM(Δ64)*(c)*[c] with NS5806	0.43	0.58	1.83	0.39
DREAM(Δ160)	0.75	0.47	2.16	0.29
DREAM(Δ160) with Mg^{2+}	0.63	0.41	2.03	0.37
DREAM(E186Q)	0.62	0.50	2.02	0.27
DREAM(E186Q) with Mg^{2+}	0.48	0.47	1.58	0.42
DREAM(E234Q)	0.63	0.27	1.75	0.46
DREAM(E234Q) with Mg^{2+}	0.45	0.31	1.70	0.48

[a] All shown parameters were recovered using a triple or double discrete exponential decay; the error of the reported values is 2.5% on average. All experiments were conducted at room temperature (~20 °C) at protein concentration of 20 μM with addition of 80 μM Tb^{3+} for CaM and 40 μM Tb^{3+} for DREAM constructs. An additional lifetime of ~80 μs was resolved for all DREAM constructs, likely due to parasitic light or PMT recovery delay, and is not shown.

[b] Measured in the presence of 131 μM TFP.

[c] The protein concentration for these experiments was 10 μM in the presence of *(a)* 100 mM NaCl, *(b)* 100 mM NaCl and 10 mM LDAO, or *(c)* 100 mM NaCl, 10 mM LDAO, and 31 μM NS5806.

Table 4

Experimental and Theoretical Ion-Neutral Collision Cross Sections for the DREAM(Δ64):Ca^{2+}/Tb^{3+} Molecular Ions

	+7 (Å^2)	+8 (Å^2)	+9 (Å^2)
theoretical[a]			
DREAM(Δ64):Ca^{2+} Ca^{2+}	2773	2798	2825
experimental			
DREAM(Δ64):Ca^{2+} Ca^{2+}	2225	2243	2297
DREAM(Δ64):Ca^{2+} Tb^{3+}	2205	2231	2260
DREAM(Δ64):Tb^{3+} Tb^{3+}	2200	2228	2238

[a]Calculated using the IMoS software as described in Materials and Methods.